Applied Catalysis B: Environmental 330 (2023) 122585

Contents lists available at ScienceDirect

Applied Catalysis B: Environmental

journal homepage: www.elsevier.com/locate/apcatb

Narrowing the bandgaps of thiazolo[5,4-*d*]thiazole-bridged conjugated microporous polymers to capture green light for selective oxidation of amines

Fengwei Huang, Xiaoyun Dong, Yuexin Wang, Xianjun Lang *

Sauvage Center for Molecular Sciences and Hubei Key Lab on Organic and Polymeric Optoelectronic Materials, College of Chemistry and Molecular Sciences, Wuhan University, Wuhan 430072, China

ARTICLE INFO

Keywords:
Benzo[1,2-b:3,4-b':5,6-b'']trithiophene
Thiazolo[5,4-*d*]thiazole
Visible light
Photocatalysis
Conjugated microporous polymers

ABSTRACT

Conjugated microporous polymers (CMPs) have evloved into versatile visible light photocatalysts. Narrowing the bandgaps of CMPs could capture more visible light without shifting the suitable position with an established electron acceptor like thiazolo[5,4-*d*]thiazole (TzTz). Here, benzene-1,3,5-tricarbaldehyde (Bz-CHO) and benzo[1,2-b:3,4-b':5,6-b'']trithiophene-2,5,8-tricarbaldehyde (BTT-CHO) are adopted to undergo condensation with dithiooxamide, preparing two TzTz-bridged CMPs, namely TzTz-Bz and TzTz-BTT. Thereby, TzTz-BTT could capture visible light more substantially than TzTz-Bz due to narrowing the bandgap. Endowed by TzTz, both TzTz-BTT and TzTz-Bz possess similar positions for the activation of O_2 and can drive the subsequent formation of imines. However, TzTz-BTT, with a narrower bandgap, could capture more green light to drive the electron and proton transfer for the selective formation of imines with higher conversions than TzTz-Bz. This work suggests that CMPs can be equipped with extensive visible light absorption for photocatalytic selective oxidations.

1. Introduction

Conjugated microporous polymers (CMPs) with extended π-conjugated skeletons and tunable linkages formed with abundant reactive groups emerge with excellent versatility [1–3]. Through unremitting efforts, CMPs have recently found applications in various domains, including catalysis [4], adsorption [5–7], sensor [8], energy storage [9], and ion separation [10]. Taken together, these applications could be the blueprint for future solar energy conversion over photoactive CMPs. With flexible underpinnings, photoactive CMPs are amenable to materials engineering in the aspect of inherent porosity, specific surface area, and band structure, which are of great importance for photocatalysis [11–13]. Thus, CMPs with adjustable bandgaps could capture visible light via the rational design of molecular units [14–16]. Besides, the extensive π-conjugation and chemical stability are beneficial to the robustness of CMPs during the course of reactions. Increasingly, CMPs with versatile functional groups have been designed and developed into efficient and stable visible light photocatalysts.

With a rigid and planar architecture, thiazolo[5,4-*d*]thiazole (TzTz) has been devoted to constructing CMPs [17–19]. Accordingly, TzTz-bridged CMPs have emerged with exceptional charge transfer and effective exciton migration [20–22]. Based on the prominent electron-deficient characteristics, distinctive TzTz-bridged CMPs could be prepared by incorporating with other moieties [23]. However, the absorption of TzTz-bridged CMPs needs to be improved and expanded [24,25]. To this end, the key of absorptive capacity lies in the choice of molecular units with extending π-conjugated skeletons and incorporating heteroatoms to narrow the bandgaps [26–29]. For aerobic oxidations, narrowing the bandgaps of TzTz-bridged CMPs could be adapted to activate O_2 with more solar light. The rational design of CMPs could widen the absorption, enabling them to capture more visible light. More important, TzTz can be formed by the direct condensation of aromatic aldehydes and dithiooxamide (DTO). Thus, aromatic skeletons with a suitable symmetry as the molecular units can narrow the bandgaps of TzTz-bridged CMPs.

Benzene-1,3,5-tricarbaldehyde (Bz-CHO), the simplest aromatic aldehyde with C_3 symmetry can form network materials. To expand the π-conjugation of benzene, the widely used planar benzo[1,2-b:3,4-b′:5,6-b′′]trithiophene (BTT) with C_3 symmetry lays the groundwork for effective intermolecular π–π interaction, which facilitates hole

* Corresponding author.
E-mail address: xianjunlang@whu.edu.cn (X. Lang).

https://doi.org/10.1016/j.apcatb.2023.122585
Received 12 December 2022; Received in revised form 15 February 2023; Accepted 4 March 2023
Available online 7 March 2023

transporting [30–32]. Thus, BTT with star-shaped π-conjugation is a molecular unit with exceptional optoelectronic properties [33]. For instance, BTT and its derivatives are electron-rich with superior photovoltaic performance and are widely used as hole-transporting materials in perovskite solar cells [34,35]. Considering this, BTT, with a rigid heteroaromatic fused ring to facilitate π-electron delocalization, is regarded as a promising candidate for photoactive CMPs [36,37]. As an established heterocycle, the potential of the π-core BTT as the electron donor has been envisaged to positively influence the activity of TzTz-bridged CMPs. Therefore, to integrate moieties of BTT and TzTz as a photocatalyst for superior aerobic oxidations, it is necessary to apply BTT core unit to narrow the bandgap of the prepared CMPs to capture more extensive visible light. Along with the narrowing of the bandgaps, the optoelectronic properties of the CMPs might shift towards more favorable positions for photocatalytic organic transformations.

In this work, with the C_3 symmetry, Bz-CHO and benzo[1,2-b:3,4-b′:5,6-b″]trithiophene-2,5,8-tricarbaldehyde (BTT-CHO) are adopted to undergo condensation with DTO, preparing the two TzTz-bridged CMPs, namely TzTz-Bz and TzTz-BTT (Fig. 1). Compared to benzene, BTT exhibits a more extensive and planar structure along with heteroatom S incorporation. The S-rich BTT is selected to prepare TzTz-BTT with extended π-conjugated structure and wide light absorption. By narrowing the bandgap, TzTz-BTT could capture visible light more substantially than TzTz-Bz. TzTz-BTT and TzTz-Bz are verified to capture visible light for selective oxidation of benzyl amines. Eventually, TzTz-BTT, with a narrower bandgap than TzTz-Bz, could capture more green light, leading to better conversions of amines to imines with O_2. This work foreshadows that CMPs with extensive visible light absorption are applicable for selective oxidations.

2. Experimental section

2.1. Materials

DTO, Bz-CHO, and BTT-CHO were purchased from Adamas. Dichloromethane (DCM) and anhydrous *N,N*-dimethylformamide (DMF) were sourced from Sinopharm Chemical Reagent Co. Ltd. Other reagents were obtained from J&K Scientific, TCI, Merck, Fischer Scientific, Sigma-Aldrich, Aladdin, Alfa Aesar, and Sinopharm Chemical Reagent Co. Ltd., etc. All the commercially available reagents were directly used without further purifications.

2.2. Preparation of the two TzTz-bridged CMPs

The preparation of the two TzTz-bridged CMPs was inspired by our prior work [38]. Firstly, DTO (27.7 mg, 0.23 mmol) and 4 mL DMF were fixed with BTT-CHO (50.8 mg, 0.153 mmol) or Bz-CHO (24.9 mg, 0.153 mmol) in a Pyrex tube to fashion TzTz-BTT and TzTz-Bz, respectively. After 5 min of ultrasonication and three cycles of degassing treatments, the Pyrex tube was sealed with flame. Subsequently, the mixtures was treated under 150 °C for 120 h and then washed by DCM and DMF. The collected solids were treated by Soxhlet extraction for 48 h with DCM and dried in a vacuum drying oven. Finally, the two TzTz-bridged CMPs were obtained as TzTz-BTT in dark red and TzTz-Bz in yellow.

2.3. Photocatalytic reaction procedure

The procedure for selective oxidation of benzylamine over TzTz-BTT is as follows. Firstly, TzTz-BTT (5 mg) and benzylamine (0.3 mmol) were immersed in acetonitrile (CH_3CN, 1 mL) and stirred for 0.5 h under darkness after 5 min of ultrasonic dispersion in a 20 mL Pyrex reactor. Then, under an O_2 atmosphere, the progress of the system in the reactor was driven by green light. Finally, the products in the supernatant were quantified with a gas chromatograph with a flame ionization detector (GC–FID). Additionally, further identification of the products was from the gas chromatography–mass spectrometry (GC–MS).

3. Results and discussion

3.1. Characterizations of the two TzTz-bridged CMPs

TzTz can be fashioned through the direct condensation of aromatic aldehyde and DTO [39,40]. First, the preparation of the two TzTz-bridged CMPs was successfully confirmed by solid-state ^{13}C nuclear magnetic resonance (NMR) spectroscopy. In the solid-state ^{13}C NMR spectra (Fig. 2), the chemical shifts at 163.2 and 167.2 ppm were ascribed to C═N in the TzTz rings. The representative signals at 150.5 and 151.1 ppm appeared to validate the presence of TzTz. The characteristic signal for C═C arose at 131.7 ppm for TzTz-BTT and 134.5 ppm for TzTz-Bz.

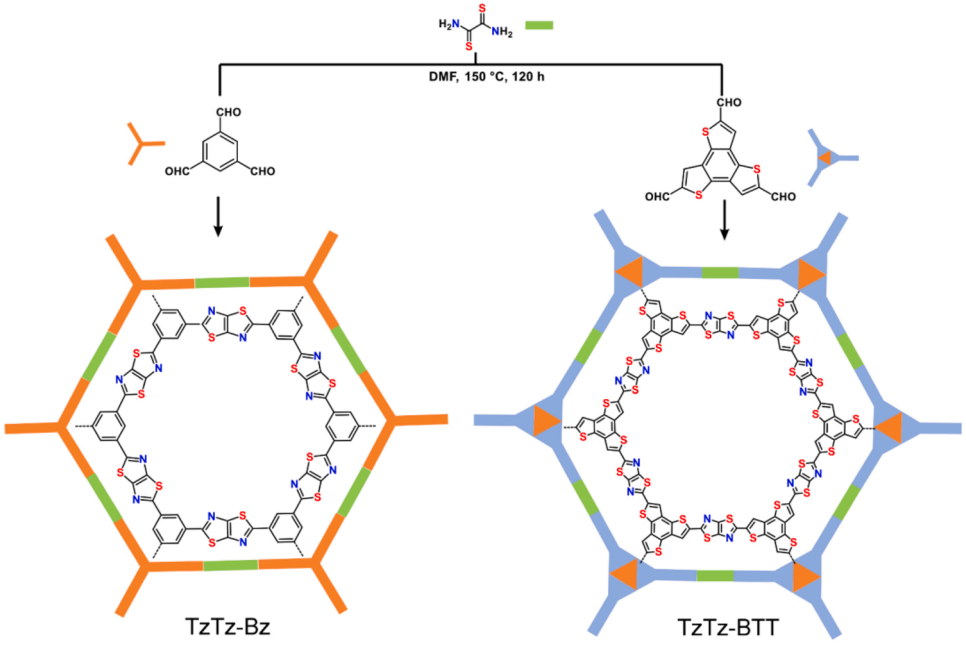

Fig. 1. The preparation of TzTz-Bz and TzTz-BTT.

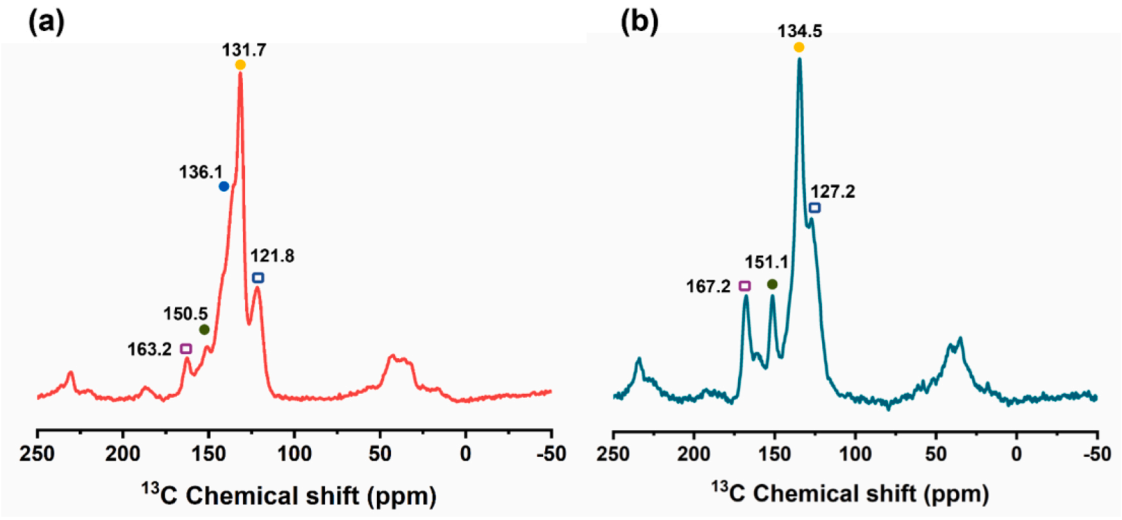

Fig. 2. The solid-state ^{13}C NMR spectra of (a) TzTz-BTT and (b) TzTz-Bz.

The formation of the two TzTz-bridged CMPs was also corroborated by Fourier transform infrared (FTIR) spectroscopy. From the FTIR spectra (Supplementary Fig. S1), both TzTz-BTT and TzTz-Bz showed waning of the peaks of C═O at 1670 and 1700 cm^{-1} compared to the monomers, which proves the condensation of aromatic aldehydes and DTO. Additionally, TzTz-Bz showed the characteristic signal at 1600 cm^{-1}, corresponding to C═N stretching band. The powder X-ray diffraction (PXRD) patterns (Supplementary Fig. S2) of TzTz-BTT and TzTz-Bz unveiled broad 2θ peaks, consistent with the amorphous characteristics of typical CMPs.

Next, the porosities of the two TzTz-bridged CMPs were investigated. Derived from N_2 sorption isotherms (Fig. 3a and b), TzTz-BTT and TzTz-Bz possessed Brunauer–Emmett–Teller (BET) specific surface areas of 412 $m^2\ g^{-1}$ and 244 $m^2\ g^{-1}$, respectively. The pore sizes of TzTz-BTT and TzTz-Bz mainly distributed around 1.18 nm and 1.27 nm (Fig. 3c and d), as calculated according to the non-local density functional

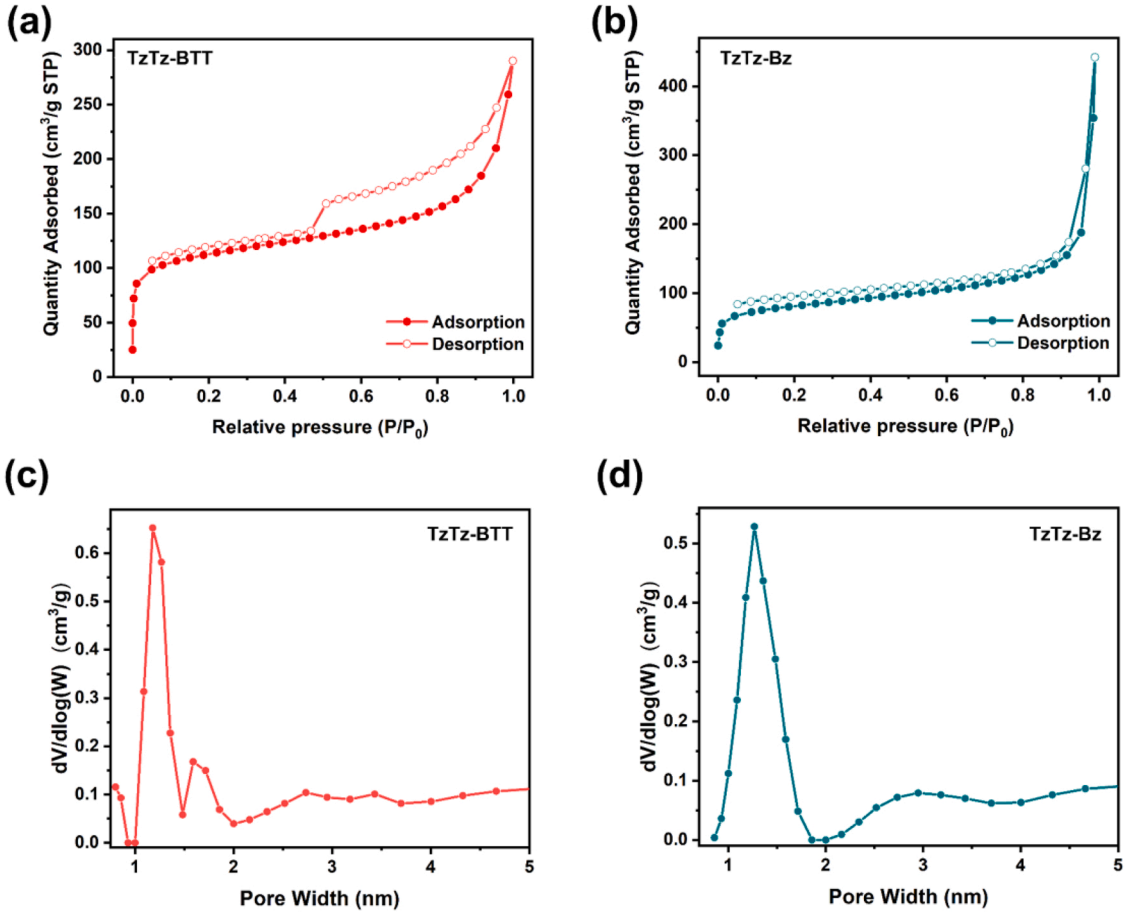

Fig. 3. N_2 sorption isotherms for (a) TzTz-BTT and (b) TzTz-Bz; Pore size distribution of (c) TzTz-BTT and (d) TzTz-Bz.

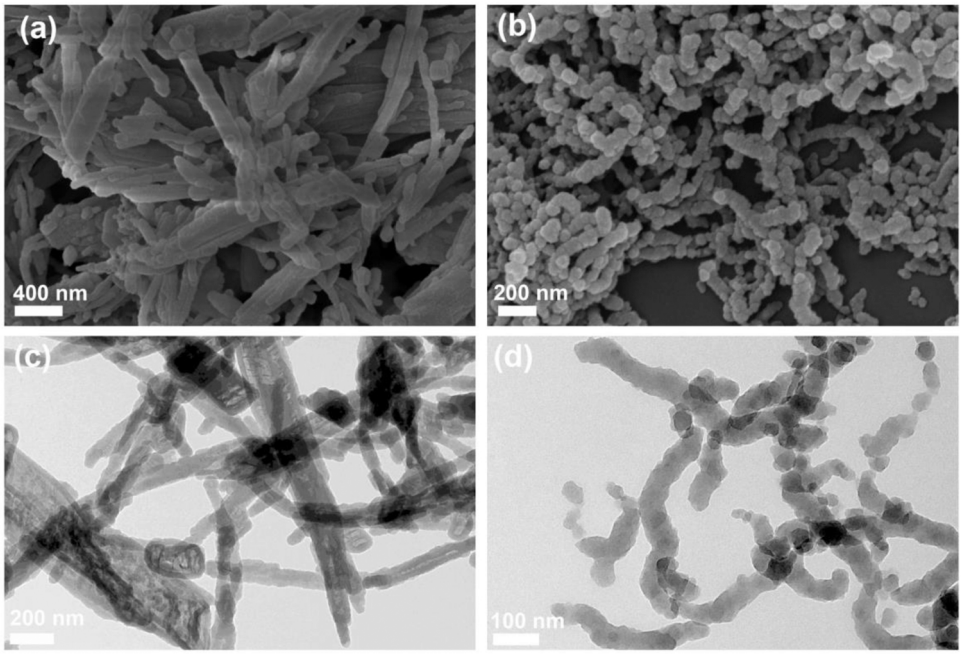

Fig. 4. SEM images of (a) TzTz-BTT and (b) TzTz-Bz; TEM images of (c) TzTz-BTT and (d) TzTz-Bz.

theory model. Additionally, TzTz-BTT and TzTz-Bz possessed dual porosities both in micropores and mesopores. No significant change in pore volume was observed and the pore volumes were 0.37 $cm^3\ g^{-1}$ for TzTz-BTT and 0.32 $cm^3\ g^{-1}$ for TzTz-Bz.

The morphologies of the two TzTz-bridged CMPs were also observed. The scanning electron microscopy (SEM) image clearly shows that TzTz-BTT was mainly composed of a rod-like structure (Fig. 4a). In contrast, TzTz-Bz revealed relatively uniform stacked worm-like aggregation in

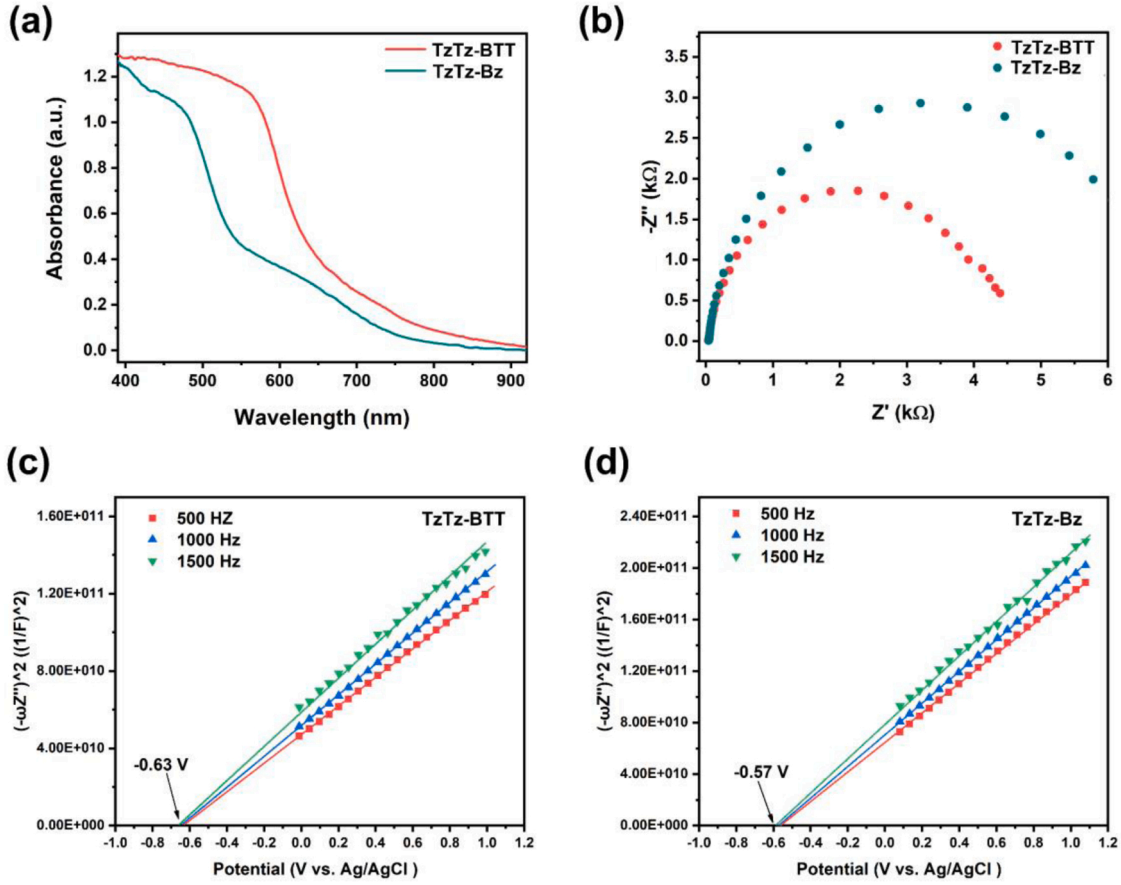

Fig. 5. (a) Solid-state UV–visible spectra; (b) EIS spectra of TzTz-BTT and TzTz-Bz; Mott–Schottky plots of (c) TzTz-BTT and (d) TzTz-Bz.

Table 1
Selective oxidation of benzylamines over TzTz-bridged CMPs driven by green light.[a]

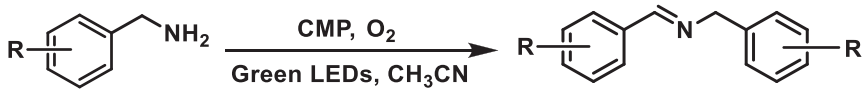

Entry	Substrate	Product	CMP	Conv. (%)[b]	Sel. (%)[b]
1	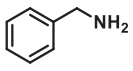	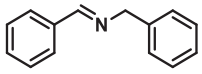	TzTz-BTT	86	99
2	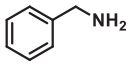	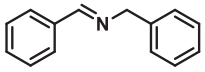	TzTz-Bz	36	88
3	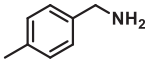	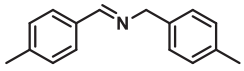	TzTz-BTT	77	99
4	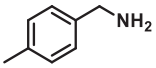	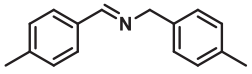	TzTz-Bz	40	85
5	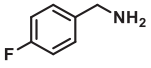	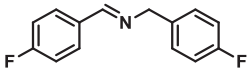	TzTz-BTT	79	99
6	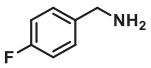	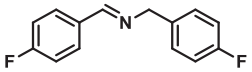	TzTz-Bz	36	91

[a] Standard reaction conditions: CMP (5 mg), benzylamine (0.3 mmol), green LEDs (520 ± 15 nm), CH_3CN (1 mL), 1.2 h, O_2 (1 atm).
[b] Detected by GC–FID, conversion of benzylamines, selectivity of the corresponding imines.

the SEM image (Fig. 4b). Transmission electron microscopy (TEM) images (Fig. 4c and d) were also collected to gather extra morphological information of TzTz-BTT and TzTz-Bz. TEM images correspond well with the SEM images. Thermogravimetric (TG) analysis is a vital tool to assess the thermal durability of the two TzTz-bridged CMPs. Therefore, the time-dependent weight change curves (Supplementary Fig. S3) of TzTz-BTT and TzTz-Bz were acquired. The two TzTz-bridged CMPs had pronounced thermal stability. Less than 10 wt% weight loss was observed below 300 °C. Notably, the weight loss of TzTz-BTT was lower than that of TzTz-Bz from 300 to 800 °C. The extended π-conjugated planes of BTT might increase the thermal stability of TzTz-BTT.

Next, the light absorptions of the two TzTz-bridged CMPs were recorded by solid-state UV–visible spectroscopy. As illuminated in Fig. 5a, TzTz-BTT had a wider absorption range than TzTz-Bz, suggesting that the extended π-conjugation and heteroatom of BTT promotes the bathochromic shift of the absorption. Unequivocally, the rational design could enable the TzTz-bridged CMPs to capture more visible light. Furthermore, the optical bandgaps for TzTz-BTT and TzTz-Bz deduced from Tauc plots (Supplementary Fig. S4) were 1.98 and 2.30 eV, respectively. In addition to a wider absorption range, TzTz-BTT reflected in a smaller arc radius than TzTz-Bz in the electrochemical impedance spectroscopy (EIS, Fig. 5b), manifesting a lower electrochemical impendence. Furthermore, transient photocurrent responses of TzTz-BTT were higher than that of TzTz-Bz (Supplementary Fig. S5), indicating the improved charge separation. Based on Fig. 5c and d, the values of flat-band potential (E_{fb}) were estimated to be −0.63 V for TzTz-BTT and −0.57 V for TzTz-Bz versus Ag/AgCl, which are sufficient for activating O_2 to superoxide ($O_2^{\bullet-}$) (−0.48 V versus Ag/AgCl). This might slightly contribute to $O_2^{\bullet-}$ yielding but could not be substantial because these are quite similar to each other. All of these observations, together with photoelectric performance tests, indicate that the two TzTz-bridged CMPs with desired structural characteristics are expected to be used in activating O_2 to reactive oxygen species (ROS) like $O_2^{\bullet-}$. Additionally, the charge transfer process after irradiation was investigated by the time-resolved fluorescence lifetime decay spectroscopy. The average fluorescence lifetime of TzTz-BTT and TzTz-Bz were quite similar (Supplementary Fig. S6). Surface topographic images and surface potential mappings of TzTz-BTT and TzTz-Bz with/without irradiation were investigated by Kelvin probe force microscopy (KPFM, Supplementary Fig. S7). The surface photopotential shift of TzTz-BTT (10 mV) was greater than that of TzTz-Bz (3 mV), indicating the larger accumulation of photogenerated charge carriers on TzTz-BTT (Supplementary Fig. S8).

Further, the electron cloud distributions of TzTz-BTT and TzTz-Bz were simulated using density functional theory (DFT) calculations at B3LYP/6–31 G(d) level (Supplementary Fig. S9). The HOMO (highest occupied molecular orbital)–LUMO (lowest unoccupied molecular orbital) energy gap value was predicted to be 2.93 eV of TzTz-BTT,

Table 2
Selective oxidation of primary amines over TzTz-BTT driven by green light.[a]

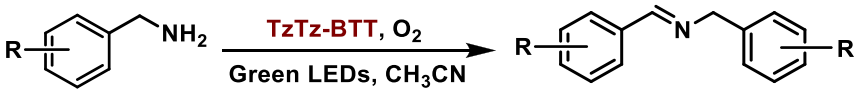

Entry	Substrate	Product	*t* (h)	Conv. (%)[b]	Sel. (%)[b]
1	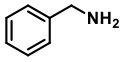	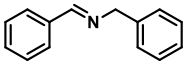	1.3	95	99
2	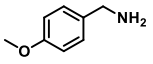	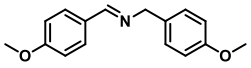	1.7	98	99
3	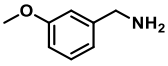	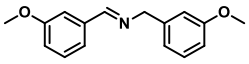	1.7	90	99
4	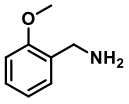	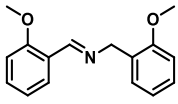	1.9	91	99
5	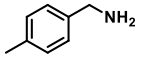	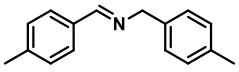	1.4	94	99
6	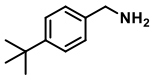	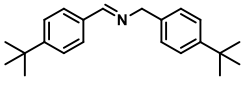	1.7	96	99
7	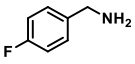	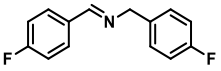	1.4	92	99
8	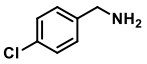	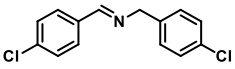	1.7	94	99
9	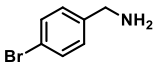	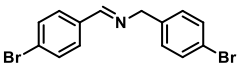	1.8	90	99
10	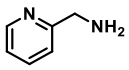	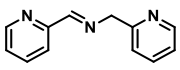	1.2	99	53
11	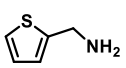	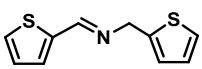	1.9	84	90

[a] Reaction conditions: TzTz-BTT (5 mg), primary amine (0.3 mmol), green LEDs (520 ± 15 nm), CH_3CN (1 mL), O_2 (1 atm).
[b] Detected by GC–FID, conversion of primary amine, selectivity of the corresponding imine.

Table 3
Selective oxidation of secondary amines to imines over TzTz-BTT driven by green light.[a]

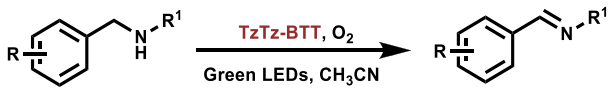

Entry	Substrate	Product	*t* (h)	Conv.(%)[b]	Sel.(%)[b]
1	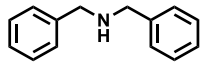	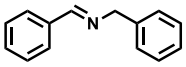	2.0	90	83
2	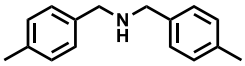	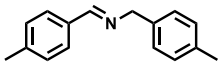	2.0	95	78
3	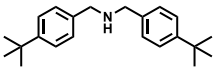	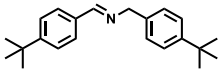	2.0	81	74
4	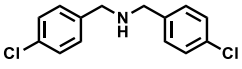	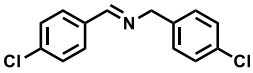	3.0	96	80
5	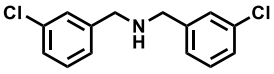	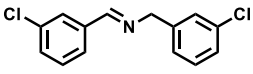	3.0	80	82
6	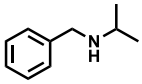	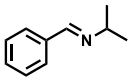	1.4	92	71

[a] Reaction conditions: TzTz-BTT (5 mg), secondary amine (0.15 mmol), green LEDs (520 ± 15 nm), CH_3CN (1 mL), O_2 (1 atm).
[b] Detected by GC–FID, conversion of secondary amine, selectivity of the corresponding imine.

narrower than that of TzTz-Bz (3.60 eV), which matches perfectly with the experimentally determined trend. The TzTz-BTT showed a clear separation of HOMOs and LUMOs in DFT results, and the LUMO orbitals are mainly localized on the acceptor unit of TzTz ring due to the donor core of BTT in the polymer skeletons. While the HOMO and LUMO orbitals TzTz-Bz are uniformly distributed on the simplified fragmental structures. Additionally, molecular electrostatic potential (ESP) maps of TzTz-BTT and TzTz-Bz were computed using the predicted densities, showing that negative potential mainly focuses on the N atoms of the TzTz ring.

3.2. Oxidation of amines over the TzTz-bridged CMPs

Solar energy has become a sustainable alternative to fossil energy that has adverse effects on the environment [41–46]. Organic transformations driven by visible light are recognized as an important arena of photocatalytic applications [47,48]. Among them, the selective oxidation of amines has been the focus of extensive investigations, and thus numerous photocatalysts have been developed to yield imine products [49–52]. Therefore, the two TzTz-bridged CMPs were applied to the selective oxidation of benzylamines driven by green light. The results show that the photocatalytic activity of TzTz-BTT was superior to TzTz-Bz, whether benzylamine or substituted benzylamines were adopted as the substrate (Table 1). TzTz-BTT, with a narrower bandgap, could capture more green light to drive the electron and proton transfer for the formation of *N*-benzylbenzaldimine in higher conversions than TzTz-Bz. It further confirms the hypothesis that the expanded π-conjugated structure and the introduction of heteroatoms in TzTz-BTT are beneficial to the photocatalytic reaction driven by green light. The comparison with the previously reported work on the conversion of benzylamine is arranged in Supplementary Table S1, implying the superiority of TzTz-BTT.

Table 2 enumerates the oxidation of a variety of primary amines over TzTz-BTT photocatalyst. The results demonstrated that TzTz-BTT is a suitable photocatalyst driven by green light. The conversions of substituted benzylamines were slower than that of benzylamines in both the electron-withdrawing and electron-donating substrates (Table 2, entries 1–9). Irrespective of the electron effect, it was not difficult to find that the steric effect can also hinder the reaction (Table 2, entries 2–4). When S or N heteroatom-containing substrate is used as a reactant, desirable outcomes are also exhibited (Table 2, entries 10 and 11). In general, different kinds of substituted substrates could be efficiently transformed with high selectivity in a short period of time, which also proves that TzTz-BTT is an ideal candidate for the efficient conversion of amines with good toleration.

The selective oxidation of secondary amines over TzTz-BTT photocatalyst was also measured to accurately establish the general applicability. The observation that kinds of secondary amines were smoothly oxidized, revealing that the transformation is affected by both electronic and steric effects (Table 3). Except for bis(4-methylbenzyl)amine, the conversions of substituted amines were inferior to the convesion of dibenzylamine (Table 3, entries 1–5). Steric effect was also revealed, in

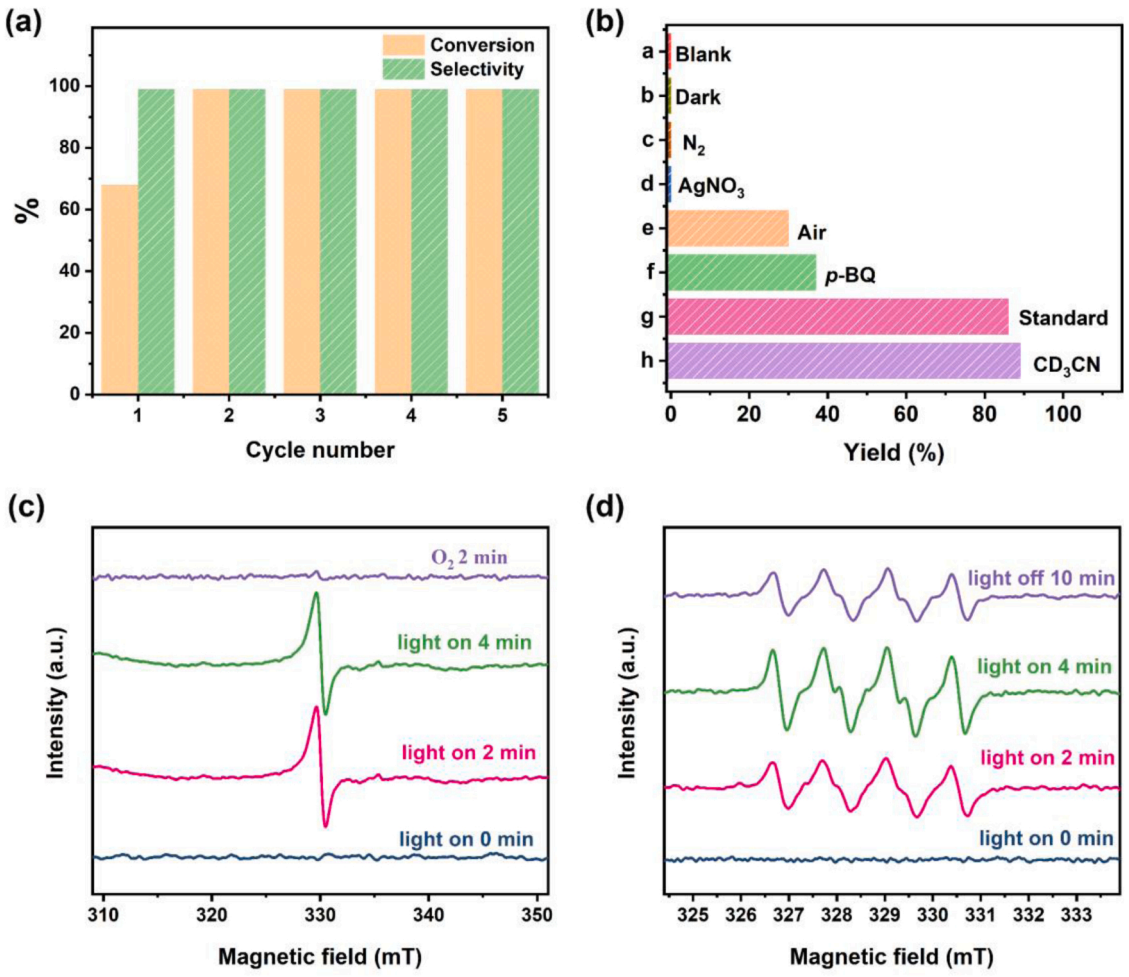

Fig. 6. (a) Recycling experiments of TzTz-BTT photocatalyst. Standard reaction conditions: TzTz-BTT (5 mg), benzylamine (0.3 mmol), green LEDs (520 ± 15 nm), CH_3CN (1 mL), 1.0 h, O_2 (1 atm). (b) Control experiments. Standard reaction conditions: TzTz-BTT (5 mg), benzylamine (0.3 mmol), green LEDs (520 ± 15 nm), CH_3CN (1 mL), 1.2 h, O_2 (1 atm). The detected EPR spectra of (c) e^- and (d) $O_2^{\bullet-}$ trapped by DMPO over TzTz-BTT.

which a noticeable drop of conversion in bis(3-chlorobenzyl)amine was observed compared with bis(4-chlorobenzyl)amine (Table 3, entries 4 and 5). In contrast, it is worth mentioning that when the electron donor group was replaced on the N atom, the reaction was effectively enhanced (Table 3, entry 6).

3.3. Reaction mechanism over TzTz-BTT photocatalyst

After establishing the feasibility, stability assessments of TzTz-BTT photocatalyst that withstand photocatalytic oxidation conditions were conducted (Fig. 6a). For practical application, the regenerability of photocatalysts is of particular significance. The results show that the oxidation of benzylamine was facilitated after one cycle. Probably, the stacked structures of TzTz-BTT were partly opened with the induction process by light irradiation, thereby modulating the photocatalytic behavior [53]. It was also reflected in the phenomenon that there was hypsochromic shift of the absorption range of TzTz-BTT after irradiation (Supplementary Fig. S10). Furthermore, it is satisfying that the oxidation efficiency of TzTz-BTT photocatalyst was not at loss even after five cycles, ensuring the possibility of regeneration. Moreover, compared with TzTz-BTT, TzTz-BTT after irradiation showed a similar FTIR spectrum with the enhanced characteristic peak of C═N at 1620 cm^{-1}, which further proves the stability of TzTz-BTT (Supplementary Fig. S11). In addition to green light, longer wavelength light could also drive the selective oxidation of benzylamine, benefiting from the wide absorption range of TzTz-BTT (Supplementary Fig. S12).

Control experiments without photocatalyst TzTz-BTT, oxidant O_2, or green light yielded no imine product (Fig. 6b, a–c), suggesting these three are prerequisites. ROS is the intermediate of the oxidant O_2 and is of importance in photocatalytic organic transformations. Verifying the predominant ROS in the oxidation processes is vital for clarifying the reaction mechanism [54–56]. To monitor the ROS over TzTz-BTT driven by green light, ROS quenching was implemented. $AgNO_3$, alongside O_2 as the acceptor for electron (e^-) prevented the formation of *N*-benzylbenzaldimine (Fig. 6b, d). When $O_2^{\bullet-}$ was captured by *p*-benzoquinone (*p*-BQ), sharp decline in yield of imine was displayed (Fig. 6b, f). Thus, $O_2^{\bullet-}$ is a predominant ROS in the transformation of benzylamine. CD_3CN is proven to lengthen the lifetime of $^1O_2$ [57]. However, the oxidation of benzylamine in CD_3CN did not increase significantly (Fig. 6b, h). All of these observations suggest that $O_2^{\bullet-}$ is the predominant ROS.

Furthermore, electron paramagnetic resonance (EPR) spectroscopy could also evidence that $O_2^{\bullet-}$ exerted aerobic oxidation. Firstly, the behavior of e^- was investigated, in which e^- is in the EPR visible for direct detection [58]. The e^- signal increased under irradiation in the absence of O_2 and decreased in the presence of O_2 (Fig. 6c). Thus, O_2 averted the accumulation of e^- driven by green light over TzTz-BTT. Fig. 6d exhibits that the 5,5-dimethyl-1-pyrroline *N*-oxide (DMPO) trapped $O_2^{\bullet-}$ signal enhanced under constant light irradiation, suggesting $O_2^{\bullet-}$ was sufficiently generated. Additionally, the signal of benzylamine radicals trapped by *N*-benzylidene-*tert*-butylamine *N*-oxide (PBN) was also detected, revealing the occurrence of benzylamine radical cation over TzTz-BTT driven by green light (Supplementary Fig. S13).

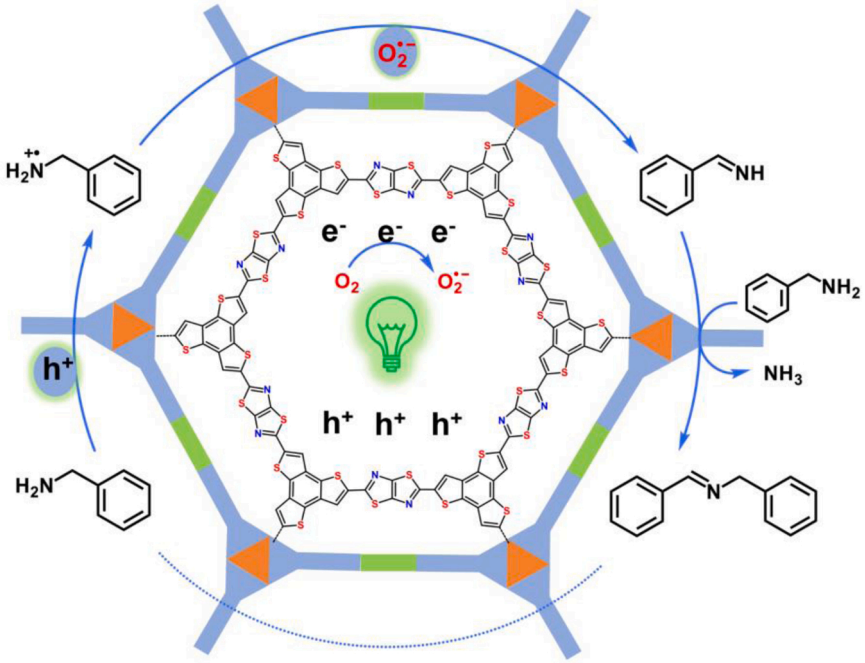

Fig. 7. A plausible mechanism of selective oxidation of benzylamine with O_2 over TzTz-BTT photocatalyst driven by green light.

In a nutshell, a plausible reaction mechanism over TzTz-BTT photocatalyst is illustrated in Fig. 7. First, green light steers to the separation of e^-–h^+ pairs over TzTz-BTT. Then, benzylamine is activated by h^+ localized at the donor BTT, generating a benzylamine radical cation. Meanwhile, O_2 intercepts e^- at the acceptor TzTz to form $O_2^{\bullet-}$. Next, benzylamine radical cation is consumed by $O_2^{\bullet-}$, being converted to benzaldimine. Ultimately, the product *N*-benzylbenzaldimine is finished by coupling with benzylamine accompanied by releasing NH_3.

4. Conclusions

In summary, two TzTz-bridged CMPs, namely TzTz-BTT and TzTz-Bz, have been designed and prepared by the direct condensation of aromatic aldehydes and DTO. TzTz, the linkages as well as the electron acceptor for the two CMPs, activated O_2 satisfactorily to ROS $O_2^{\bullet-}$. To narrow the bandgaps, the π-conjugation of the electron donor was extended by shifting from benzene to BTT, alongside the incorporation of S, leading to the superior light absorption of TzTz-BTT to that of TzTz-Bz. As a result, TzTz-BTT could more sufficiently capture green light for the oxidation of amines with O_2. Essentially, $O_2^{\bullet-}$ gave rise to the formation of imines. Notably, TzTz-BTT photocatalyst preserved activity after five cycles due to the robustness of TzTz and BTT. Besides, TzTz-BTT was of general applicability for the photocatalytic selective oxidation of amines driven by green light. This work provides new insights into designing CMPs to capture extensive visible light for photocatalysis.

CRediT authorship contribution statement

Fengwei Huang: Investigation, Formal analysis, Writing – original draft. **Xiaoyun Dong**: Investigation, Formal analysis. **Yuexin Wang**: Investigation, Formal analysis. **Xianjun Lang**: Conceptualization, Supervision, Writing – review & editing, Funding acquisition.

Declaration of Competing Interest

The authors declare that they have no known competing financial interests or personal relationships that could have appeared to influence the work reported in this paper.

Data availability

Data will be made available on request.

Acknowledgments

This work was supported by the National Natural Science Foundation of China (Grants 22072108 and 21773173). The numerical calculations were done on the supercomputing system in the Supercomputing Center of Wuhan University. We also acknowledge the Core Facility of Wuhan University for materials characterizations.

Appendix A. Supplementary material

Supplementary data associated with this article can be found in the online version at doi:10.1016/j.apcatb.2023.122585.

References

[1] J.M. Lee, A.I. Cooper, Advances in conjugated microporous polymers, Chem. Rev. 120 (2020) 2171–2214, https://doi.org/10.1021/acs.chemrev.9b00399.
[2] W.Y. Zhang, H.Y. Zuo, Z.H. Cheng, Y. Shi, Z.J. Guo, N. Meng, A. Thomas, Y.Z. Liao, Macroscale conjugated microporous polymers: Controlling versatile functionalities over several dimensions, Adv. Mater. 34 (2022), 2104952, https://doi.org/10.1002/adma.202104952.
[3] G. Xiang, X.S. He, Y.X. Liu, Q. Huang, W. Huang, C.Z. Zhang, J.Y. Peng, A sensitive photoelectrochemical sensor for levodopa detection using benzothiadiazole-based conjugated microporous polymer-coated graphene heterostructures, ACS Appl. Mater. Interfaces 14 (2022) 51329–51340, https://doi.org/10.1021/acsami.2c15516.
[4] S.H. Ryu, S.M. Lee, H.J. Kim, Y.J. Ko, K.C. Ko, S.U. Son, Concomitant shape and palladium engineering of hollow conjugated microporous photocatalysts to boost visible light-induced hydrogen evolution, J. Mater. Chem. A 9 (2021) 22262–22268, https://doi.org/10.1039/d1ta06498c.
[5] L. Ma, Y.L. Liu, Y. Liu, S.Y. Jiang, P. Li, Y.C. Hao, P.P. Shao, A.X. Yin, X. Feng, B. Wang, Ferrocene-linkage-facilitated charge separation in conjugated microporous polymers, Angew. Chem. Int. Ed. 58 (2019) 4221–4226, https://doi.org/10.1002/anie.201813598.
[6] J.Z. Xu, W. Xie, C. Yao, G.J. Xu, S.R. Zhang, Y.H. Xu, Preparation of sulfur-containing conjugated microporous polymer for adsorbing iodine and Fe^{3+} sensing, J. Environ. Chem. Eng. 9 (2021), 106399, https://doi.org/10.1016/j.jece.2021.106399.
[7] L. Zhang, N. Pu, B.X. Yu, G. Ye, J. Chen, S.M. Xu, S.Q. Ma, Skeleton engineering of homocoupled conjugated microporous polymers for highly efficient uranium

capture via synergistic coordination, ACS Appl. Mater. Interfaces 12 (2020) 3688–3696, https://doi.org/10.1021/acsami.9b20944.
[8] H.Q. Liu, Y. Wang, W.Q. Mo, H.L. Tang, Z.Y. Cheng, Y. Chen, S.T. Zhang, H.W. Ma, B. Li, X.B. Li, Dendrimer-based, high-luminescence conjugated microporous polymer films for highly sensitive and selective volatile organic compound sensor arrays, Adv. Funct. Mater. 30 (2020), 1910275, https://doi.org/10.1002/adfm.201910275.
[9] S.B. Ren, W.Y. Ma, C. Zhang, L. Chen, K. Wang, R.R. Li, M. Shen, D.M. Han, Y. X. Chen, J.X. Jiang, Exploiting polythiophenyl-triazine-based conjugated microporous polymer with superior lithium-storage performance, ChemSusChem 13 (2020) 2295–2302, https://doi.org/10.1002/cssc.202000200.
[10] Z.Y. Zhou, D. Guo, D.B. Shinde, L. Cao, Z. Li, X. Li, D.W. Lu, Z.P. Lai, Precise sub-angstrom ion separation using conjugated microporous polymer membranes, ACS Nano 15 (2021) 11970–11980, https://doi.org/10.1021/acsnano.1c03194.
[11] T. Zhang, G.L. Xing, W.B. Chen, L. Chen, Porous organic polymers: A promising platform for efficient photocatalysis, Mater. Chem. Front. 4 (2020) 332–353, https://doi.org/10.1039/c9qm00633h.
[12] C.H. Dai, B. Liu, Conjugated polymers for visible-light-driven photocatalysis, Energy Environ. Sci. 13 (2020) 24–52, https://doi.org/10.1039/c9ee01935a.
[13] C.Z. Han, S.H. Xiang, M.T. Ge, P.X. Xie, C. Zhang, J.X. Jiang, An efficient electron donor for conjugated microporous polymer photocatalysts with high photocatalytic hydrogen evolution activity, Small 18 (2022), 2202072, https://doi.org/10.1002/smll.202202072.
[14] J. Xiao, X.L. Liu, X.K. Gao, J.H. Hu, L. Pan, C.X. Shi, X.W. Zhang, J.J. Zou, Controllable construction of alkynyl defective dibenzo[b,d]thiophene-sulfone-based conjugated microporous polymers for enhanced photocatalytic performance, J. Catal. 414 (2022) 155–162, https://doi.org/10.1016/j.jcat.2022.09.003.
[15] J. Xiao, X.L. Liu, L. Pan, C.X. Shi, X.W. Zhang, J.J. Zou, Heterogeneous photocatalytic organic transformation reactions using conjugated polymers-based materials, ACS Catal. 10 (2020) 12256–12283, https://doi.org/10.1021/acscatal.0c03480.
[16] S.Z. Li, W.J. Zhang, S. Yang, F. Chen, C.Y. Pan, J.T. Tang, K.A.I. Zhang, G.P. Yu, Phenothiazine-based conjugated microporous polymers: Pore surface and bandgap engineering for visible light-driven aerobic oxidative cyanation, Chem. Eng. J. 408 (2021), 127261, https://doi.org/10.1016/j.cej.2020.127261.
[17] M.M. Sany, I.M.A. Mekhemer, M.G. Mohamed, M.H. Elsayed, K.H. Lin, Y.K. Chen, T.L. Wu, H.H. Chou, Conjugated microporous polymers incorporating thiazolo[5,4-d]thiazole moieties for sunlight-driven hydrogen production from water, Chem. Eng. J 446 (2022), 137158, https://doi.org/10.1016/j.cej.2022.137158.
[18] M. Samal, S. Valligatla, N.A. Saad, M.V. Rao, D.N. Rao, R. Sahu, B.P. Biswal, A thiazolo[5,4-*d*]thiazole-bridged porphyrin organic framework as a promising nonlinear optical material, Chem. Commun. 55 (2019) 11025–11028, https://doi.org/10.1039/c9cc05415d.
[19] B.P. Biswal, D. Becker, N. Chandrasekhar, J.S. Seenath, S. Paasch, S. Machill, F. Hennersdorf, E. Brunner, J.J. Weigand, R. Berger, X.L. Feng, Exploration of thiazolo[5,4-*d*]thiazole linkages in conjugated porous organic polymers for chemoselective molecular sieving, Chem. Eur. J. 24 (2018) 10868–10875, https://doi.org/10.1002/chem.201802631.
[20] Y.C. Wang, H. Liu, Q.Y. Pan, N.X. Ding, C.M. Yang, Z.H. Zhang, C.C. Jia, Z.B. Li, J. Liu, Y.J. Zhao, Construction of thiazolo[5,4-*d*]thiazole-based two-dimensional network for efficient photocatalytic CO_2 reduction, ACS Appl. Mater. Interfaces 12 (2020) 46483–46489, https://doi.org/10.1021/acsami.0c12173.
[21] A.F. Saber, A.M. Elewa, H.H. Chou, A.F.M. El-Mahdy, Donor-acceptor carbazole-based conjugated microporous polymers as photocatalysts for visible-light-driven H_2 and O_2 evolution from water splitting, Appl. Catal., B 316 (2022), 121624, https://doi.org/10.1016/j.apcatb.2022.121624.
[22] C.L. Chang, A.M. Elewa, J.H. Wang, H.H. Chou, A.F.M. El-Mahdy, Donor-acceptor conjugated microporous polymers based on thiazolo[5,4-*d*]thiazole building block for high-performance visible-light-induced H_2 production, Microporous Mesoporous Mater. 345 (2022), 112258, https://doi.org/10.1016/j.micromeso.2022.112258.
[23] G. Sathiyan, R. Ranjan, S. Ranjan, A. Garg, R.K. Gupta, A. Singh, Dicyanovinylene and thiazolo[5,4-*d*]thiazole core containing D–A–D type hole-transporting materials for spiro-ometad-free perovskite solar cell applications with superior atmospheric stability, ACS Appl. Energy Mater. 2 (2019) 7609–7618, https://doi.org/10.1021/acsaem.9b01598.
[24] Q. Huang, L.P. Guo, N. Wang, X. Zhu, S.B. Jin, B.E. Tan, Layered thiazolo [5,4-*d*] thiazole-linked conjugated microporous polymers with heteroatonn adoption for efficient photocatalysis application, ACS Appl. Mater. Interfaces 11 (2019) 15861–15868, https://doi.org/10.1021/acsami.8b21765.
[25] G. Gryn'ova, C. Corminboeuf, Implications of charge penetration for heteroatom-containing organic semiconductors, J. Phys. Chem. Lett. 7 (2016) 5198–5204, https://doi.org/10.1021/acs.jpclett.6b02585.
[26] R.S. Sprick, C.M. Aitchison, E. Berardo, L. Turcani, L. Wilbraham, B.M. Alston, K. E. Jelfs, M.A. Zwijnenburg, A.I. Cooper, Maximising the hydrogen evolution activity in organic photocatalysts by co-polymerisation, J. Mater. Chem. A 6 (2018) 11994–12003, https://doi.org/10.1039/c8ta04186e.
[27] B. Kan, H.R. Feng, X.J. Wan, F. Liu, X. Ke, Y.B. Wang, Y.C. Wang, H.T. Zhang, C. X. Li, J.H. Hou, Y.S. Chen, Small-molecule acceptor based on the heptacyclic benzodi(cyclopentadithiophene) unit for highly efficient nonfullerene organic solar cells, J. Am. Chem. Soc. 139 (2017) 4929–4934, https://doi.org/10.1021/jacs.7b01170.
[28] S.X. Dai, Y.Q. Xiao, P.R. Xue, J.J. Rech, K. Liu, Z.Y. Li, X.H. Lu, W. You, X.W. Zhan, Effect of core size on performance of fused-ring electron acceptors, Chem. Mater. 30 (2018) 5390–5396, https://doi.org/10.1021/acs.chemmater.8b02222.
[29] B.Y. Jia, S.X. Dai, Z.F. Ke, C.Q. Yan, W. Ma, X.W. Zhan, Breaking 10% efficiency in semitransparent solar cells with fused-undecacyclic electron acceptor, Chem. Mater. 30 (2018) 239–245, https://doi.org/10.1021/acs.chemmater.7b04251.
[30] X.F. Wu, W.J. Wang, H. Hang, H. Li, Y.H. Chen, Q. Xu, H. Tong, L.X. Wang, Star-shaped fused-ring electron acceptors with a C_{3h}-symmetric and electron-rich benzotri(cyclopentadithiophene) core for efficient nonfullerene organic solar cells, ACS Appl. Mater. Interfaces 11 (2019) 28115–28124, https://doi.org/10.1021/acsami.9b08017.
[31] J. Calbo, R. Viruela, J. Aragó, E. Ortí, Theoretical insights into the structural, electronic and optical properties of benzotrithiophene-based hole-transporting materials, Theor. Chem. Acc. 136 (2017) 73, https://doi.org/10.1007/s00214-017-2100-4.
[32] Z.Z. Sun, S. Feng, C.T. Gu, N.A. Cheng, J.F. Liu, Probing effects of molecular conformation on the electronic and charge transport properties in two- and three-dimensional small molecule hole-transporting materials: A theoretical investigation, Phys. Chem. Chem. Phys. 21 (2019) 15206–15214, https://doi.org/10.1039/c9cp01986c.
[33] Y. Wang, W.D. Xu, J.P. Yi, C. Zuo, Y.T. Gong, Y.Y. Liu, W.Y. Lai, W. Huang, Improving the exciton dissociation of polymer/fullerene interfaces with a minimal loading amount of energy cascading molecular dopant, J. Mater. Chem. A 6 (2018) 18325, https://doi.org/10.1039/c8ta90205d.
[34] Y.K. Peng, K.M. Lee, C.C. Ting, M.W. Hsu, C.Y. Liu, Making benzotrithiophene derivatives dopant-free for perovskite solar cells: Step-saving installation of π-spacers by a direct C–H arylation strategy, J. Mater. Chem. A 7 (2019) 24765–24770, https://doi.org/10.1039/c9ta09777e.
[35] I. García-Benito, I. Zimmermann, J. Urieta-Mora, J. Aragó, A. Molina-Ontoria, E. Ortí, N. Martín, M.K. Nazeeruddin, Isomerism effect on the photovoltaic properties of benzotrithiophene-based hole-transporting materials, J. Mater. Chem. A 5 (2017) 8317–8324, https://doi.org/10.1039/c7ta00997f.
[36] S.J. Han, Z.P. Li, S. Ma, Y.F. Zhi, H. Xia, X. Chen, X.M. Liu, Bandgap engineering in benzotrithiophene-based conjugated microporous polymers: A strategy for screening metal-free heterogeneous photocatalysts, J. Mater. Chem. A 9 (2021) 3333–3340, https://doi.org/10.1039/d0ta10232f.
[37] X.W. Pan, C.H. Ding, Z.M. Zhang, H.Z. Ke, G.E. Cheng, Functional porous organic polymer with high S and N for reversible iodine capture, Microporous Mesoporous Mater. 300 (2020), 110161, https://doi.org/10.1016/j.micromeso.2020.110161.
[38] X. Li, X.M. Ma, F.L. Zhang, X.Y. Dong, X.J. Lang, Selective photocatalytic formation of sulfoxides by aerobic oxidation of sulfides over conjugated microporous polymers with thiazolo[5,4-*d*]thiazole linkage, Appl. Catal., B 298 (2021), 120514, https://doi.org/10.1016/j.apcatb.2021.120514.
[39] M. Saito, I. Osaka, Impact of side chain placement on thermal stability of solar cells in thiophene-thiazolothiazole polymers, J. Mater. Chem. C 6 (2018) 3668–3674, https://doi.org/10.1039/c7tc04721e.
[40] A.N. Woodward, J.M. Kolesar, S.R. Hall, N.A. Saleh, D.S. Jones, M.G. Walter, Thiazolothiazole fluorophores exhibiting strong fluorescence and viologen-like reversible electrochromism, J. Am. Chem. Soc. 139 (2017) 8467–8473, https://doi.org/10.1021/jacs.7b01005.
[41] X.Y. Qiu, Y. Zhang, Y.F. Zhu, C. Long, L.N. Su, S.Q. Liu, Z.Y. Tang, Applications of nanomaterials in asymmetric photocatalysis: Recent progress, challenges, and opportunities, Adv. Mater. 33 (2021), 2001731, https://doi.org/10.1002/adma.202001731.
[42] Z. Wang, C. Li, K. Domen, Recent developments in heterogeneous photocatalysts for solar-driven overall water splitting, Chem. Soc. Rev. 48 (2019) 2109–2125, https://doi.org/10.1039/c8cs00542g.
[43] D.D. Li, M. Kassymova, X.C. Cai, S.Q. Zang, H.L. Jiang, Photocatalytic CO_2 reduction over metal-organic framework-based materials, Coord. Chem. Rev. 412 (2020) 213262, https://doi.org/10.1016/j.ccr.2020.213262.
[44] J.J. Rueda-Marquez, I. Levchuk, P. Fernández Ibañez, M. Sillanpää, A critical review on application of photocatalysis for toxicity reduction of real wastewaters, J. Clean. Prod. 258 (2020), 120694, https://doi.org/10.1016/j.jclepro.2020.120694.
[45] J.H. Kim, J.S. Lee, Elaborately modified $BiVO_4$ photoanodes for solar water splitting, Adv. Mater. 31 (2019), 1806938, https://doi.org/10.1002/adma.201806938.
[46] J. Liu, N.K. Ma, W. Wu, Q.G. He, Recent progress on photocatalytic heterostructures with full solar spectral responses, Chem. Eng. J. 393 (2020), 124719, https://doi.org/10.1016/j.cej.2020.124719.
[47] R. Li, J. Byun, W. Huang, C. Ayed, L. Wang, K.A.I. Zhang, Poly(benzothiadiazoles) and their derivatives as heterogeneous photocatalysts for visible-light-driven chemical transformations, ACS Catal. 8 (2018) 4735–4750, https://doi.org/10.1021/acscatal.8b00407.
[48] T. Banerjee, F. Podjaski, J. Kroger, B.P. Biswal, B.V. Lotsch, Polymer photocatalysts for solar-to-chemical energy conversion, Nat. Rev. Mater. 6 (2021) 168–190, https://doi.org/10.1038/s41578-020-00254-z.
[49] P.Q. Chen, Z.F. Guo, X. Liu, H. Lv, Y. Che, R. Bai, Y.H. Chi, H.Z. Xing, A visible-light-responsive metal–organic framework for highly efficient and selective photocatalytic oxidation of amines and reduction of nitroaromatics, J. Mater. Chem. A 7 (2019) 27074–27080, https://doi.org/10.1039/c9ta10723a.
[50] B. Dutta, L.A. Achola, R. Clarke, V. Sharma, J.K. He, P. Kerns, S.L. Suib, Photocatalytic transformation of amines to imines by meso-porous copper sulfides, ChemCatChem 11 (2019) 4262–4265, https://doi.org/10.1002/cctc.201900673.
[51] H.J. Chen, L.M. Peng, Y.C. Bian, X.Q. Shen, J. Li, H.C. Yao, S.Q. Zang, Z.J. Li, Exerting charge transfer to stabilize Au nanoclusters for enhanced photocatalytic performance toward selective oxidation of amines, Appl. Catal., B 284 (2021), 119704, https://doi.org/10.1016/j.apcatb.2020.119704.

[52] J.L. Shi, R.F. Chen, H.M. Hao, C. Wang, X.J. Lang, 2D sp^2 carbon-conjugated porphyrin covalent organic framework for cooperative photocatalysis with TEMPO, Angew. Chem. Int. Ed. 59 (2020) 9088–9093, https://doi.org/10.1002/anie.202000723.
[53] Y.X. Wang, X. Li, X.Y. Dong, F.L. Zhang, X.J. Lang, Triazine-based two dimensional porous materials for visible light-mediated oxidation of sulfides to sulfoxides with O_2, J. Colloid Interface Sci. 616 (2022) 846–857, https://doi.org/10.1016/j.jcis.2022.02.114.
[54] Y. Nosaka, A.Y. Nosaka, Generation and detection of reactive oxygen species in photocatalysis, Chem. Rev. 117 (2017) 11302–11336, https://doi.org/10.1021/acs.chemrev.7b00161.
[55] X.R. Li, Y. Chen, Y. Tao, L. Shen, Z.M. Xu, Z.F. Bian, H.X. Li, Challenges of photocatalysis and their coping strategies, Chem Catal. 2 (2022) 1315–1345, https://doi.org/10.1016/j.checat.2022.04.007.
[56] Y. Chen, M.J. Xu, J.Y. Wen, Y. Wan, Q.F. Zhao, X. Cao, Y. Ding, Z.L. Wang, H.X. Li, Z.F. Bian, Selective recovery of precious metals through photocatalysis, Nat. Sustainability 4 (2021) 618–626, https://doi.org/10.1038/s41893-021-00697-4.
[57] M. Bregnhøj, M. Westberg, F. Jensen, P.R. Ogilby, Solvent-dependent singlet oxygen lifetimes: Temperature effects implicate tunneling and charge-transfer interactions, Phys. Chem. Chem. Phys. 18 (2016) 22946–22961, https://doi.org/10.1039/c6cp01635a.
[58] K.M. Kareh, In situ electron paramagnetic resonance spectroscopy for catalysis, Nat. Rev. Methods Prim. 1 (2021) 34, https://doi.org/10.1038/s43586-021-00036-z.